Check for updates

physica status solidi (a)

RESEARCH ARTICLE OPEN ACCESS

High Resolution Temperature-Resolved Spectroscopy of the Nitrogen-Vacancy ^{1}E Singlet State Ionization Energy

Kristine V. Ung[1,2,3] | Connor A. Roncaioli[4] | Ronald L. Walsworth[1,2,3,5] | Sean M. Blakley[4]

[1]Department of Physics, University of Maryland, College Park, Maryland, USA | [2]Joint Quantum Institute, University of Maryland, College Park, Maryland, USA | [3]Quantum Technology Center, University of Maryland, College Park, Maryland, USA | [4]DEVCOM Army Research Laboratory, Adelphi, Maryland, USA | [5]Department of Electrical Engineering, University of Maryland, College Park, Maryland, USA

Correspondence: Sean M. Blakley (sean.m.blakley2.civ@army.mil)

Received: 30 June 2025 | **Revised:** 8 January 2026 | **Accepted:** 11 January 2026

Keywords: defects | diamond | quantum optics | spectroscopy

ABSTRACT

The negatively charged diamond nitrogen-vacancy (NV^-) center plays a central role in many quantum sensing applications, though much is still unknown about the energy levels in this system. The ionization energy of the ^{1}E singlet state in the NV^- center has only recently been measured to be between 2.25 and 2.33 eV. In this work, we reduce this uncertainty by measuring the ^{1}E ionization energy as a function of excitation laser wavelength and diamond temperature via magnetically mediated spin-selective photoluminescence (PL) quenching that transfers population from the ^{1}E in the NV^- into the neutral NV^0 charge configuration. Measurements are performed for excitation wavelengths between 450 and 470 nm, and between 540 and 566 nm in increments of 2 nm, and for temperatures ranging from about 50 to 150 K in 5 K increments. We determine the ^{1}E ionization energy to be between 2.29 and 2.33 eV, which provides about a twofold reduction in uncertainty of this quantity. Distribution level: A. Approved for public release; distribution unlimited.

1 | Introduction

The nitrogen-vacancy (NV) center in diamond is a highly effective quantum sensor due to its good thermal properties [1–3], stable fluorescence [4], and high spin contrast [5], making it a sensitive and adaptable measurement tool for a variety of applications [6, 7]. Understanding the energy level structure of the NV center is critical for quantum sensing with the NV center, enabling the development of measurement techniques like spin-to-charge conversion and photoelectric detection of magnetic resonance (PDMR) that possess a higher contrast and signal count rate relative to typical fluorescence sensing [5, 8–11]. The ^{1}E singlet state in the negative NV charge configuration (NV^-) is of key importance to optically detected magnetic resonance (ODMR) quantum sensing with the NV center, and yet it remains the least well understood of the known energy levels. Previous work on this subject has shown, via direct photoionization, that the ionization energy of the ^{1}E is between 2.25 and 2.33 eV [12]. These measurements were performed with a combination of gas, dye, and solid state lasers, and possessed an average wavelength resolution of approximately 13 nm and an average temperature resolution of approximately 50 K. This course resolution left a large uncertainty in the measured value of the ^{1}E ionization energy. In this manuscript, we report a twofold reduction in the uncertainty in the ^{1}E ionization energy by measuring photoluminescence (PL) spectra over two wavelength ranges, 450–470 and 540–566 nm, with 2 nm wavelength increments. Measurements are performed at two laser powers of 0.1 and 1.0 mW, and at 5 K temperature steps from 50 to 150 K.

2 | Experimental Section

The NV^- charge configuration has four electronic spin states, which include the triplet ground state ($^3A_2$) and the triplet excited

This is an open access article under the terms of the Creative Commons Attribution License, which permits use, distribution and reproduction in any medium, provided the original work is properly cited.

© 2026 The Author(s). *physica status solidi (a)* applications and materials science published by Wiley-VCH GmbH. This article has been contributed to by U.S. Government employees and their work is in the public domain in the USA.

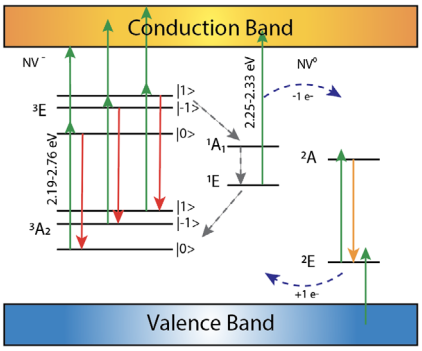


FIGURE 1 | Energy level diagram of the nitrogen-vacancy system in the negative (NV^-) and neutral (NV^0) charge configurations. Solid straight arrows indicate transitions mediated by one photon, whereas dashed straight arrows indicate transitions mediated primarily by phonons. Curved dashed arrows indicate transitions between charge configurations.

state (^3E) which both possess a $S=1$ spin [13–15], as well as a singlet ($S=0$) excited state ($^1A_1$) and the metastable ^1E singlet state. When optically illuminating the system with wavelengths between 470 and 637 nm, an NV absorbs a photon and transitions from $^3A_2$ to ^3E while conserving electronic spin. The system can either relax back to $^3A_2$ via photon emission or into $^1A_1$ via the upper intersystem crossing (ISC) and then into ^1E. The transition into ^1E via the upper ISC and $^1A_1$ is a nonradiative process in the visible wavelength band. For the $m_z=\pm1$ spin sublevels of ^3E, relaxation to ^1E via the upper ISC is more likely than relaxation to ^1E from the $m_z=0$ spin sublevel of the ^3E. The decay rate back to $^3A_2$ from ^1E via the lower ISC is relatively slow, giving the ^1E a lifetime that is an order of magnitude larger than any other NV^- state besides the $^3A_2$ ground state [16]. Under suitable optical illumination, these processes lead to the preparation of the NV^- electronic spin state into $m_z=0$, and also allow the NV^- spin state to be readout via PL measurement (Figure 1). While the photophysics of most NV^- states is well established [17, 18] ^1E ionization is the subject of debate in the literature [19–23], with the ^1E ionization energy only recently determined [12, 24–29].

To measure the ^1E ionization energy, a wavelength-resolved direct photoionization method was previously developed [12]. This method involves applying a bias magnetic field of at least 100 mT, aligned approximately along the diamond [001] axis, so that the $m_s=0$ and $m_s=-1$ spin sublevels [30–32] in the ^3E triplet excited state are mixed for NV^- centers along all four diamond crystallographic axes. This choice of a bias field magnitude applied along the [001], [010], or [100] (demonstrated previously using a field oriented perpendicular to the square surface of the diamond sample [12]) directions ensures a significant increase in the ^1E population via its ISC with ^3E, resulting in a measurable enhancement in NV^0 PL due to ^1E photoionization. The orientation of the field along the [001] axis in this work allows the diamond plate to lie flat on the sample holder between the magnetic field poles.

2.1 | Measurement Procedure

The present work employs an expanded version of the method used in Ref. [12]. The procedure for measuring the ^1E energy proceeds in two steps. The first step involves recording a reference PL spectrum from the NV^- centers with no bias magnetic field, and optical illumination from one candidate ionization wavelength (Figure 2a). This PL spectrum defines the reference measurement, creating a steady-state charge configuration ratio between NV^- and NV^0 at the applied ionization wavelength for a system with negligible ^1E population. Due to the lack of population in ^1E, the only photoionization pathways available to the NV system for this combination of experimental parameters are either direct single photoionization from the $^3A_2$ triplet ground state to the conduction band [13, 17] for sufficiently large ionization energies, or two-photon Auger ionization proceeding from $^3A_2$ to the conduction band via the ^3E triplet state for lower ionization energies [17]. The second step involves recording a PL spectrum with an applied magnetic field of about 100 mT for the same ionization wavelength as the reference measurement. The bias field induces mixing of the ^3E $|0\rangle$ and $|-1\rangle$ spin states, thus more readily populating the ^1E sublevel so that the system may ionize from there [12] (Figure 2b,c), opening an additional two-photon ionization pathway for the NV system. In this second step, the system proceeds from $^3A_2$ to ^3E via one photon

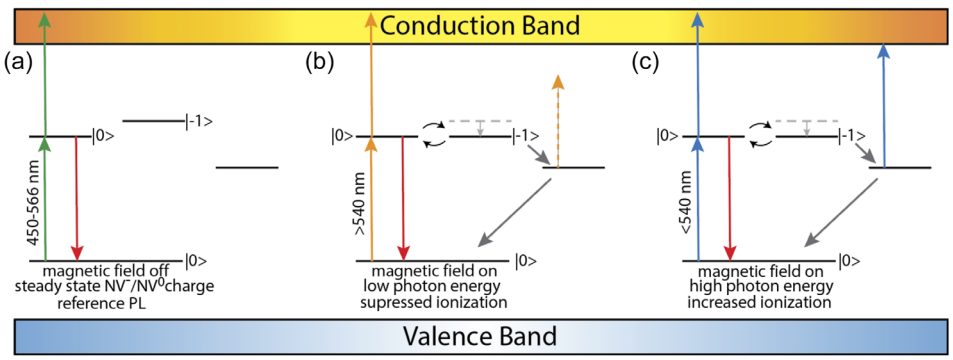


FIGURE 2 | Ionization measurement sequence for spectroscopic analysis of the ^1E singlet state. (a) Bias magnetic field off reference PL measurement compared to field on signal measurement (b,c). (b) If the photon energy is less than the ^1E ionization threshold, ^1E protects ^3E from Auger ionization, leading to decreased NV^0 PL output relative to the reference. (c) If the photon energy is greater than the ^1E ionization threshold, ^1E ionizes in addition to ^3E, leading to increased NV^0 PL output relative to the reference.

18626319, 2026, 6, Downloaded from https://onlinelibrary.wiley.com/doi/10.1002/pssa.202500538 by Ronald Walsworth , Wiley Online Library on [16/03/2026]. See the Terms and Conditions (https://onlinelibrary.wiley.com/terms-and-conditions) on Wiley Online Library for rules of use; OA articles are governed by the applicable Creative Commons License

absorption and then decays to ^{1}E via the upper ISC with ^{3}E. Once in ^{1}E, the NV$^-$ can either ionize via absorption of a second photon of sufficient energy, or remain in ^{1}E (and later decay to $^3A_2$) if the second photon energy is too small to trigger ionization.

If the photon energy (i.e., illumination wavelength) is insufficient for NV$^-$ ionization from the ^{1}E state, then ^{1}E occupancy protects the NV$^-$ from two-photon Auger ionization by reducing the steady-state population in the ^{3}E state during optical illumination (Figure 2b) in a process typically referred to as "^{1}E shelving". This shelving mechanism shifts the charge configuration ratio in favor of NV$^-$, reducing the contribution of NV^0 to the measured PL spectrum in comparison to the reference PL spectrum. If the photon energy is sufficient to ionize the ^{1}E, this results in an additional increase in the NV^0 population, resulting in a larger contribution to the measured PL spectrum when compared to the reference PL spectrum measured in the first step (Figure 2c).

2.2 | Experimental Apparatus

A Hübner C-Wave laser is used to induce ^{1}E ionization of an ensemble of NV$^-$ centers in the diamond sample (Figure 3). The laser consists of an oven-controlled, periodically polled lithium niobate (PPLN) nonlinear crystal in a bow-tie cavity with an in-line etalon. This cavity is pumped by the second-harmonic output of a 5 W diode-pumped frequency doubled Nd:YAG laser, forming an optically parametric oscillator (OPO) that is continuously tunable within two bands in the infrared (IR), from 900 to 1040 nm and from 1080 to 1300 nm. Wavelength tuning is accomplished by pumping the PPLN crystal at the polling period index associated with the desired output band, adjusting the PPLN crystal oven temperature to tune the output within the band selected by the polling period, and filtering the resulting output wavelengths with the in-line etalon.

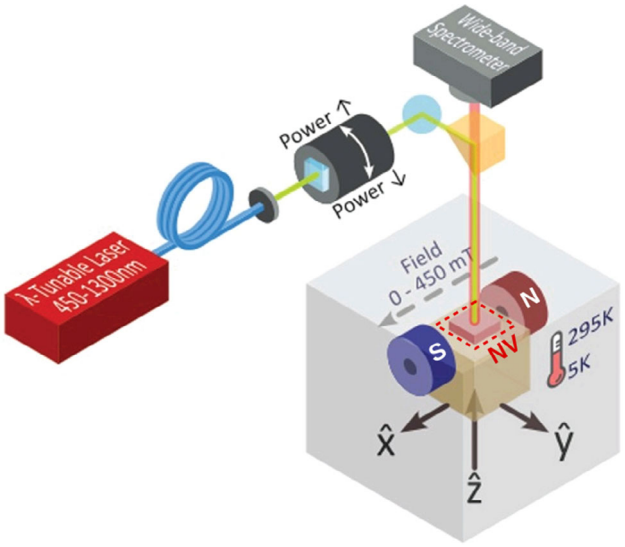


FIGURE 3 | Experimental apparatus for measuring the ionization threshold of the NV ^{1}E state, consisting of a wavelength tunable continuous wave (CW) laser, a mechanical laser power tuner, a temperature controlled cryostat with three-axis translation stage and optical access, a tunable uniaxial bias magnetic field, an NV diamond sample, a wide-band low-noise optical spectrometer, and associated optical elements.

Once locked to the desired IR wavelength, the OPO output light enters a second bowtie cavity where it is frequency doubled by an additional oven-controlled second-harmonic generation (SHG) PPLN crystal. The combined optical output of the OPO and SHG system is thereby continuously tunable from 450 to 520 nm and from 540 to 650 nm in the visible wavelength band, with a dead region between 520 and 540 nm around the 532 nm pump wavelength. The tuned SHG output is coupled to a polarization maintaining (PM) fiber as it exits the C-Wave laser module.

After tuning the laser output to the desired wavelength, the laser power is stabilized by a Glan-Taylor polarizer mounted inside a stepper-motorized rotation stage at the output of the PM fiber. The resulting wavelenght tuned laser output is then sampled by a 10% pick-off beam splitter and coupled to a diode power meter for monitoring. The laser power stabilizer unit is controlled by a software module that rotates the polarizer to tune the power output to the user specified setpoint as read by the power meter, and then continuously adjusts the power once every 25 ms to keep the laser power within $\pm 0.25\%$ of the power setpoint value.

The wavelength and power tuned laser output then proceeds through a pair of steering mirrors and is reflected off a 570 nm long pass filter into a 10x long working distance optical objective focused through the input viewport at the top of a Montana Instruments cryostat and onto the NV$^-$ diamond sample. The diamond sample (CVD grown by Element Six) is a 3 mm × 3 mm × 0.5 mm quantum grade diamond, isotopically enriched to 99.99% ^{12}C content, with defects homogeneously distributed throughout the entire sample volume and relevant defect concentrations of [N] ≈ 16 ppm and [NV] ≈4 ppm. The diamond plate is polished so that the top face is along the [100] direction. The diamond is mounted on top of a three-axis Attocube piezo stack that moves the diamond into the focal point of the objective, with the diamond's [100] axis facing up, and between the poles of a controllable uniaxial electromagnet whose field is both approximately uniform between the magnet poles and aligned to within 1° of angular displacement from the diamond's [001] axis (max field of ± 450 mT). The magnetic field magnitude and cryostat temperature are controlled by a software module that tunes both the field and temperature to user specified set points. The PL signal from the diamond is collected by the optical objective and directed through the 570 nm long pass filter into the fiber input of a Ocean Optics QE Pro low-noise wide-band spectrometer with a bandwidth between 350 and 1140 nm. PL spectra are collected for an exposure time of 100 ms and averaged 10 times before being saved by a software module for further analysis.

Signal and reference PL spectral pairs are collected for every combination of laser powers of 0.1 mW and 1 mW, and wavelengths from 450 to 470 nm and from 540 to 566 nm, in 2 nm increments. Every combination of laser power and wavelength is also measured as a function of diamond temperature at 5 K increments between 50 and 150 K, for a total of 1050 PL spectral pairs across 21 diamond temperatures, 25 laser wavelengths, and 2 laser powers. The wavelength accuracy for the laser when measured by a wavemeter was approximately 0.5 nm and the maximum thermal drift of the sample stage when measured by a built-in thermocouple over the duration of each spectral pair measurement, was less than 1 K.

18626319, 2026, 6, Downloaded from https://onlinelibrary.wiley.com/doi/10.1002/pssa.202500538 by Ronald Walsworth , Wiley Online Library on [16/03/2026]. See the Terms and Conditions (https://onlinelibrary.wiley.com/terms-and-conditions) on Wiley Online Library for rules of use; OA articles are governed by the applicable Creative Commons License

3 | Results & Discussion

The measured NV^0 PL amplitude is directly proportional to the relative NV^0 population [12], and therefore serves as the primary experimental metric used to distinguish changes in NV charge configuration ratio resulting from different experimental settings. Unlike the Bayesian analysis technique highlighted in previous work [12], the analysis method in this manuscript does not explicitly separate the full measured PL spectra into separate NV^- and NV^0 PL spectra. The present method leverages the fact that there is a region of the full PL spectrum between 575 and 605 nm in which the the NV^- PL amplitude is negligible but the NV^0 PL amplitude is appreciable. By taking the ratio of the full measured PL spectrum in the bias field on configuration to the full spectrum in the field off configuration (called the ratio spectrum), amplitude changes in the NV^0-only spectral region resulting from the application of the bias magnetic field result in a change of that same spectral region the ratio spectrum. This method is used in the present study because the Bayesian analysis method [12] fails when the PL signal-to-noise ratio in the NV^0 spectral region is low for samples with less NV^0 centers due to the relative concentration of other defects like the substitutional nitrogen (P1) center [23]. Furthermore, the ratio spectrum method uses less computational resources and thus runs more quickly than the Bayesian method, which requires the calculation of multiple double integrals and employs advanced statistical methods on large arrays of possible model parameters.

The ratio spectrum in the wavelength region between 575 and 605 nm (the NV^0 band) becomes greater than one when the NV^0 PL contribution is increased in the signal spectrum relative to the reference spectrum. Given that the only experimental difference between the signal spectrum and the reference spectrum is the presence or absence of the bias magnetic field, changes in the ratio spectrum directly correspond to changes in the ratio of NV charge configuration populations (NV^0 and NV^-). A ratio spectrum of greater than one in the NV^0 band implies increased NV^0 population when the bias field is on, indicating that ^{1}E ionization is occurring. Conversely, when the ratio spectrum is less than one in the NV^0 band, ionization is not occurring due to ^{1}E shelving. When the ratio is near unity, the ionization behavior is indeterminant.

We define C_{NV^0} in Equation (1) as the normalized ^{1}E ionization contrast for a given combination of experimental settings, where $I_{on}(I_{off})$ is the arithmetic mean of the measured NV^0 PL for the bias field on (field off) setting over the NV^0 band (between 575 and 605 nm): positive values of C_{NV^0} that are at least one standard deviation above zero indicate ionization suppression due to the ^{1}E state protecting the NV^- charge configuration from Auger ionization (i.e., ^{1}E shelving); negative values of C_{NV^0} greater than one standard deviation below zero indicate ^{1}E ionization; and C_{NV^0} values that are within one standard deviation of zero are considered indeterminant ^{1}E ionization behavior.

$$C_{NV^0} = 1 - \overline{I_{on}}/\overline{I_{off}} \tag{1}$$

C_{NV^0} is determined from measured signal and reference PL spectral pairs for every combination of diamond temperature, laser wavelength, and laser power. Representative measured PL spectral pairs (Figure 4a,c,e) and their associated C_{NV^0} values (Figure 4b,d,f) demonstrate C_{NV^0} greater than, less than, and approximately equal to zero, respectively. A similar determination is made for the normalized ^{1}E ionization contrast parameter C_{NV^-}, derived from the measured NV^- PL over the NV^- band between 680 and 740 nm, as shown in Figure 4b,d,f.

C_{NV^0} values determined as in Figure 4 are plotted as a function of temperature over wavelength bands from 450 to 470 nm and 540 to 566 nm (Figure 5a,c and b,d, respectively); and for laser powers of 0.1 mW and 1 mW (Figure 5a,b and c,d, respectively). Values of C_{NV^0} more than two standard deviations greater or less than zero are interpreted as temperature and wavelength regions corresponding to strong ^{1}E shelving (Figure 5 larger dark red circles) or ionization (Figure 5 larger dark blue circles), respectively; whereas values of C_{NV^0} that are between one and two standard deviations greater or less than zero represent regions of weaker ^{1}E shelving (Figure 5 smaller pale red circles) or ionization (Figure 5 smaller pale blue circles), respectively. Regions where C_{NV^0} is within one standard deviation of zero have indeterminant ionization or shelving behavior (Figure 5 tiny gray circles). For laser powers of 0.1 mW (Figure 5a,b), a few regions of strong ^{1}E ionization occur at the edge of the triplet ionization threshold near 470 nm (2.63 eV) for temperatures above 100 K. Further, (Figure 5d) shows trends of ^{1}E ionization being heavily suppressed between 540 nm (2.29 eV) and 566 nm (2.19 eV). At 1.0 mW laser power, there is evidence of strong ^{1}E ionization near the edge of the triplet ionization threshold at most temperatures between 50 and 150 K (Figure 5c). For wavelengths between 540 and 566 nm, ^{1}E shelving dominates at all temperatures (Figure 5d), indicating almost no ionization of the ^{1}E for wavelengths longer than 540 nm in this temperature range, with the exception of measurements for laser wavelengths of 548 and 566 nm at temperatures of 95 and 150 K, respectively. The anomalous data point at 548 nm likely results from laser power drift during the measurement sequence, as discussed in the appendix below. The physical mechanism underlying the anomalous data point at 566 nm is undetermined and will be further investigated in future work.

The combined weight of these measurements considerably narrows the region of uncertainty for the onset of ^{1}E ionization from between 532 nm (2.33 eV) and 550 nm (2.25 eV) demonstrated in previous work [12] (Figure 5b,d shaded gray region) to between 532 nm (2.33 eV) and 540 nm (2.29 eV) for diamond temperatures between 50 and 150 K. The upper energy bound of 2.33 eV is taken from previous work [12] and the lower energy bound of 2.29 eV corresponds to the long wavelength edge of the natural dead band in the wavelength tunable laser used in this experiment. This new result represents a twofold reduction in uncertainty compared to Ref. [12], where the uncertainty in the Ref. [12] result is defined as the two excitation wavelengths between which C_{NV^0} changed from ionizing to shelving, indicating that the ionization threshold is somewhere between those two excitation wavelengths.

4 | Conclusion

By measuring the ratio between NV PL spectra measured with and without a 100 mT bias magnetic field and for several temperatures (50–150 K), laser excitation wavelengths (450–470 and 540–566 nm), and laser powers (0.1 and 1.0 mW), we find the

18626319, 2026, 6, Downloaded from https://onlinelibrary.wiley.com/doi/10.1002/pssa.202500538 by Ronald Walsworth , Wiley Online Library on [16/03/2026]. See the Terms and Conditions (https://onlinelibrary.wiley.com/terms-and-conditions) on Wiley Online Library for rules of use; OA articles are governed by the applicable Creative Commons License

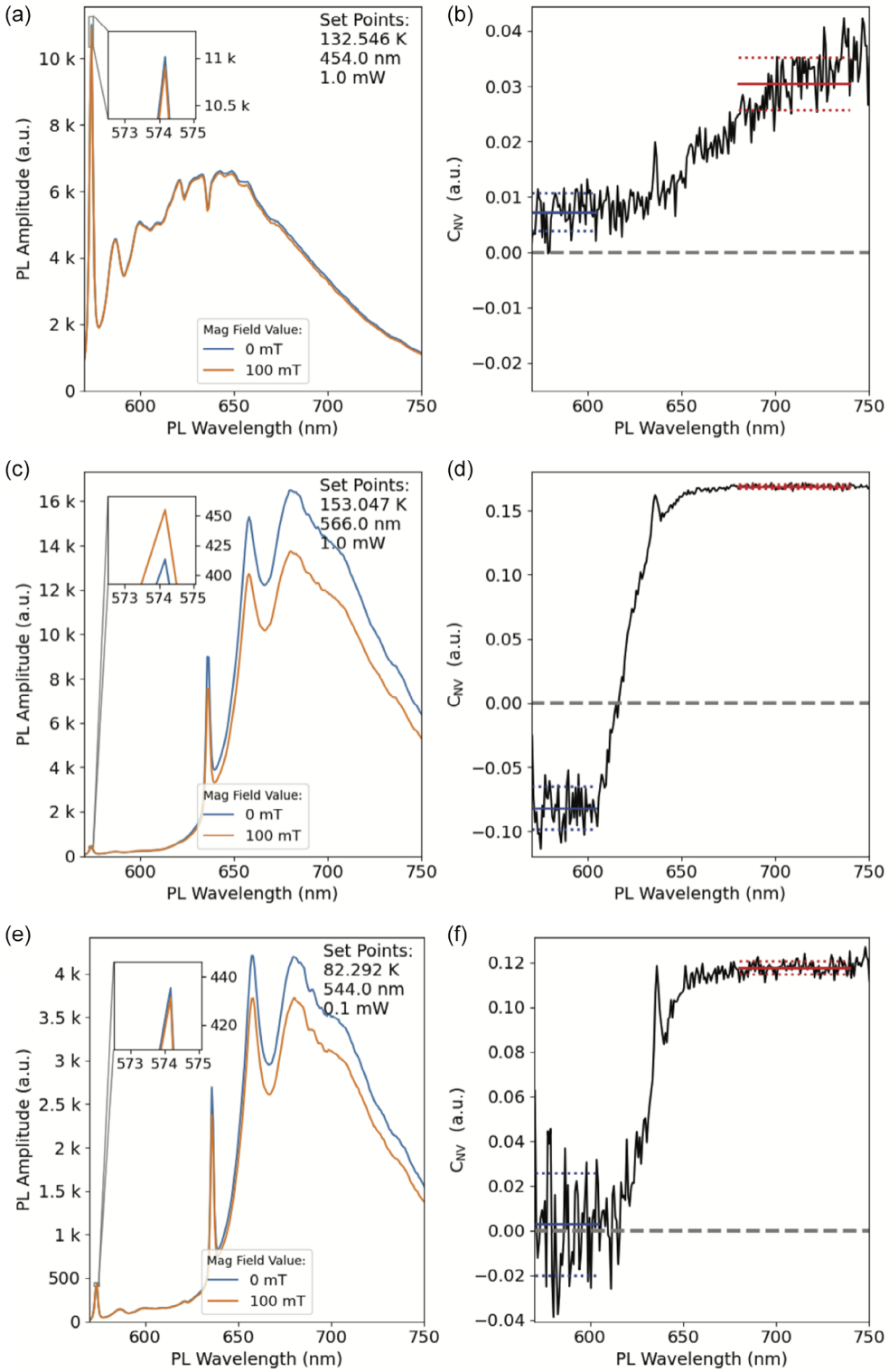


FIGURE 4 | Representative measured PL spectral pairs (bias field on and off) in (a), (c), and (e) for indicated experimental conditions, and their calculated C_{NV} values (black traces) for conditions where $C_{NV^0} > 0$, $C_{NV^0} < 0$, and $C_{NV^0} \approx 0$, in (b), (d), and (f), respectively. Solid (dashed) horizontal blue and red lines correspond to mean values (1 standard deviation) for C_{NV^0} and C_{NV^-} PL contrast, respectively. C_{NV^0} (C_{NV^-}) and their standard deviations are calculated by taking the arithmetic mean and the sample standard deviation of C_{NV^0} (C_{NV^-}) values whose wavelengths fall within the region bounded by the width of the blue (red) horizontal lines in the NV0 (NV^-) wavelength band from 575 to 605 nm (680 to 740 nm). For $C_{NV^0} > 0$, $C_{NV^0} < 0$, and $C_{NV^0} \approx 0$, the associated spectral pairs demonstrate decreased, increased, and mostly unchanged PL in the NV^0 band; this behavior is highlighted in the inset figures in (a), (c), and (e). All results show the expected reduced PL in the NV^- band due to increased population in the ^1E singlet state.

18626319, 2026, 6, Downloaded from https://onlinelibrary.wiley.com/doi/10.1002/pssa.202500538 by Ronald Walsworth , Wiley Online Library on [16/03/2026]. See the Terms and Conditions (https://onlinelibrary.wiley.com/terms-and-conditions) on Wiley Online Library for rules of use; OA articles are governed by the applicable Creative Commons License

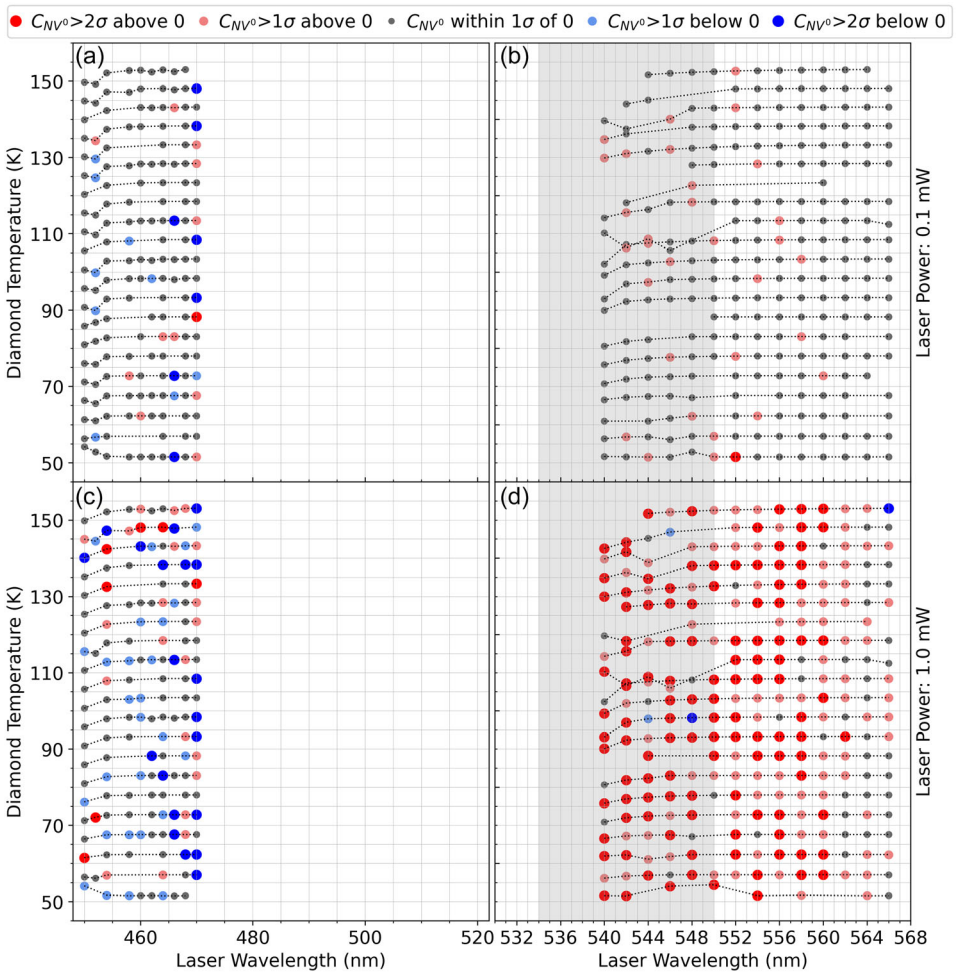


FIGURE 5 | C_{NV^0} as a function of temperature and wavelength for laser power 0.1 mW (a), (b) and 1.0 mW (c), (d) over wavelength bands from 450 to 470 nm (a), (c), and 540 to 566 nm (b), (d). Red circles indicate strong (large dark colored circles) or weak (small light colored circles) ^{1}E shelving where C_{NV^0} is greater than two standard deviations or greater than one but less than two standard deviations above zero, respectively. Small gray circles indicate that C_{NV^0} is less than one standard deviation above or below zero, corresponding to indeterminate shelving or ionization behavior. Blue circles indicate strong (large dark colored circles) or weak (small light colored circles) ^{1}E ionization where C_{NV^0} is greater than two standard deviations or greater than one but less than two standard deviations below zero respectively. Dotted gray horizontal traces indicate measurements taken within a given cryostat temperature setpoint. Gray shaded region in (b), (d) indicates the region of uncertainty for ^{1}E ionization energy determined in Ref. [12].

^{1}E ionization energy to be between 2.29 and 2.33 eV, representing a twofold reduction in the uncertainty of this quantity. This result further resolves the range of energies needed for direct spin-to-charge conversion from the ^{1}E singlet, which is a well-known tool for improving the performance of quantum sensors that rely on optically detected or PDMR measurement techniques. Planned follow-up studies include measurement at additional laser powers using the PL quenching method and a combined theoretical and experimental investigation of Jahn–Teller effects on ^{1}E ionization.

Acknowledgement

The authors would like to acknowledge many helpful scientific discussions with Robert D. McMichael during the course of this work. This material is based on work by K.V.U. supported by a Joint Quantum Institute (JQI) graduate fellowship. This work is supported by, or in part by, the U.S. Army Research Laboratory, under Contract No. W911NF2420143; the U.S. Air Force Office of Scientific Research under grant no. FA9550- 22-1-0312; and the University of Maryland Quantum Technology Center. All references to commercial devices do not constitute an endorsement by the US Government or the Army Research Laboratory; they are provided in the interest of completeness and reproducibility. The views, opinions, and/or findings expressed are those of the authors and should not be interpreted as representing the official views or policies of the Department of Defense or the U.S. Government.

Funding

This work was supported by Joint Quantum Institute; Army Research Laboratory (W911NF2420143); U.S. Air Force Office of Scientific Research (FA9550- 22-1-0312); and University of Maryland Quantum Technology Center.

Conflicts of Interest

The authors declare no conflicts of interest.

Data Availability Statement

The data that support the findings of this study are available on request from the corresponding author. The data are not publicly available due to privacy or ethical restrictions.

18626319, 2026, 6, Downloaded from https://onlinelibrary.wiley.com/doi/10.1002/pssa.202500538 by Ronald Walsworth , Wiley Online Library on [16/03/2026]. See the Terms and Conditions (https://onlinelibrary.wiley.com/terms-and-conditions) on Wiley Online Library for rules of use; OA articles are governed by the applicable Creative Commons License

References

1. A. M. Wojciechowski, M. Karadas, C. Osterkamp, et al., "Precision Temperature Sensing in the Presence of Magnetic Field Noise and vice-versa using Nitrogen-Vacancy Centers in Diamond," *Applied Physics Letters* 113, no. 1 (2018): 013502.

2. M. Yang, Q. Yuan, J. Gao, et al., "A Diamond Temperature Sensor Based on the Energy Level Shift of Nitrogen-Vacancy Color Centers," *Nanomaterials* 9, no. 11 (2019): 1576.

3. S. M. Blakley, A. B. Fedotov, J. Becker, et al., "Stimulated Fluorescence Quenching in Nitrogen–Vacancy Centers of Diamond: Temperature Effects," *Optics Letters* 41, no. 9 (2016): 2077.

4. I. V. Fedotov and A. M. Zheltikov, "Background-Free Two-Photon Fluorescence Readout via a Three-Photon Charge-State Modulation of Nitrogen Vacancy Centers in Diamond," *Optics Letters* 44, no. 15 (2019): 3737, publisher: Optica Publishing Group.

5. J. F. Barry, J. M. Schloss, E. Bauch, et al., "Sensitivity Optimization for NV-Diamond Magnetometry," *Reviews of Modern Physics* 92, no. 1 (2020): 015004.

6. R. Schirhagl, K. Chang, M. Loretz, and C. L. Degen, "Nitrogen-Vacancy Centers in Diamond: Nanoscale Sensors for Physics and Biology," *Annual Review of Physical Chemistry* 65, no. 1 (2014): 83.

7. M. Doherty, C. Meriles, A. Alkauskas, H. Fedder, M. Sellars, and N. Manson, "Towards a Room-Temperature Spin Quantum Bus in Diamond via Electron Photoionization, Transport, and Capture," *Physical Review X* 6, no. 4 (2016): 041035.

8. E. Bourgeois, A. Jarmola, P. Siyushev, et al., "Photoelectric Detection of Electron Spin Resonance of Nitrogen-Vacancy Centres in Diamond," *Nature Communications* 6, no. 1 (2015): 8577.

9. E. Bourgeois, E. Londero, K. Buczak, et al., "Enhanced Photoelectric Detection of NV Magnetic Resonances in Diamond under Dual-Beam Excitation," *Physical Review B* 95, no. 4 (2017): 041402.

10. E. Bourgeois, M. Gulka, and M. Nesladek, "Photoelectric Detection and Quantum Readout of Nitrogen-Vacancy Center Spin States in Diamond," *Advanced Optical Materials* 8, no. 12 (2020): 1902132.

11. E. Bourgeois, J. Soucek, J. Hruby, M. Gulka, and M. Nesladek, "Photoelectric Detection of Nitrogen-Vacancy Centers Magnetic Resonances in Diamond: Role of Charge Exchanges with Other Optoelectricaly Active Defects," *Advanced Quantum Technologies* 5, no. 5 (2022): 2100153.

12. S. M. Blakley, T. T. Mai, S. J. Moxim, et al., "Spectroscopy of Photoionization from the ^{1}E Singlet State in Nitrogen-Vacancy Centers in Diamond," *Physical Review B* 110 (2024): 134109.

13. M. W. Doherty, N. B. Manson, P. Delaney, F. Jelezko, J. Wrachtrup, and L. C. Hollenberg, "The Nitrogen-Vacancy Colour Centre in Diamond," *Physics Reports* 528, no. 1 (2013): 1.

14. Á. Gali, "Recent Advances in the ab Initio Theory of Solid-State Defect Qubits," *Nanophotonics* 12, no. 3 (2023): 359.

15. F. Jelezko and J. Wrachtrup, "Single Defect Centres in Diamond: A Review," *Physica Status Solidi A* 203, no. 13 (2006): 3207.

16. V. M. Acosta, A. Jarmola, E. Bauch, and D. Budker, "Optical Properties of the Nitrogen-Vacancy Singlet Levels in Diamond," *Physical Review B* 82, no. 20 (2010): 201202.

17. N. Aslam, G. Waldherr, P. Neumann, F. Jelezko, and J. Wrachtrup, "Photo-Induced Ionization Dynamics of the Nitrogen Vacancy Defect in Diamond Investigated by Single-Shot Charge State Detection," *New Journal of Physics* 15, no. 1 (2013): 013064.

18. K. Beha, A. Batalov, N. B. Manson, R. Bratschitsch, and A. Leitenstorfer, "Optimum Photoluminescence Excitation and Recharging Cycle of Single Nitrogen-Vacancy Centers in Ultrapure Diamond," *Physical Review Letters* 109, no. 9 (2012): 097404.

19. M. L. Goldman, M. W. Doherty, A. Sipahigil, et al., "Erratum: State-Selective Intersystem Crossing in Nitrogen-Vacancy Centers," *Physical Review B* 96, no. 3 (2017): 039905.

20. M. Goldman, A. Sipahigil, M. Doherty, et al., "Phonon-Induced Population Dynamics and Intersystem Crossing in Nitrogen-Vacancy Centers," *Physical Review Letters* 114, no. 14 (2015): 145502.

21. M. L. Goldman, M. W. Doherty, A. Sipahigil, et al., "State-Selective Intersystem Crossing in Nitrogen-Vacancy Centers," *Physical Review. B* 91, no. 16 (2015): 165201.

22. D. M. Toyli, D. J. Christle, A. Alkauskas, B. B. Buckley, C. G. Van de Walle, and D. D. Awschalom, "Measurement and Control of Single Nitrogen-Vacancy Center Spins above 600 K," *Physical Review X* 2, no. 3 (2012): 031001.

23. N. B. Manson, M. Hedges, M. S. J. Barson, et al., "NV^{-}–N^{+} Pair Centre in 1b Diamond," *New Journal of Physics* 20, no. 11 (2018): 113037.

24. S. A. Wolf, I. Meirzada, G. Haim, and N. Bar-Gill,"Nitrogen-Vacancy Singlet Manifold Ionization Energy," *Physical Review Applied* 19 (2023): 034076.

25. L. Razinkovas, M. Maciaszek, F. Reinhard, M. W. Doherty, and A. Alkauskas, "Photoionization of Negatively Charged NV Centers in Diamond: Theory and ab Initio Calculations," *Physical Review B* 104, no. 23 (2021): 235301.

26. D. Aude Craik, P. Kehayias, A. Greenspon, et al., "Microwave-Assisted Spectroscopy Technique for Studying Charge State in Nitrogen-Vacancy Ensembles in Diamond," *Physical Review Applied* 14, no. 1 (2020): 014009.

27. L. Hacquebard and L. Childress, "Charge-State Dynamics During Excitation and Depletion of the Nitrogen-Vacancy Center in Diamond," *Physical Review. A, Atomic, Molecular, and Optical Physics* 97, no. 6 (2018): 063408.

28. M. Bockstedte, F. Schütz, T. Garratt, V. Ivády, and A. Gali, "Ab initio Description of Highly Correlated States in Defects for Realizing Quantum bits," *npj Quantum Materials* 3, no. 1 (2018): 31.

29. G. Thiering and A. Gali, "Theory of the Optical Spin-Polarization Loop of the Nitrogen-Vacancy Center in Diamond," *Physical Review B* 98, no. 8 (2018): 085207.

30. S. Ernst, P. J. Scheidegger, S. Diesch, L. Lorenzelli, and C. L. Degen, "Temperature Dependence of Photoluminescence Intensity and Spin Contrast in Nitrogen-Vacancy Centers," *Physical Review Letters* 131 (2023): 086903.

31. S. Ernst, P. J. Scheidegger, S. Diesch, and C. L. Degen, "Modeling temperature-dependent population dynamics in the excited state of the nitrogen-vacancy center in diamond,," *Physical Review B* 108 (2023): 085203.

32. T. Chakraborty, R. Bhattacharya, V. Anjusha, M. Nesladek, D. Suter, and T. Mahesh, "Magnetic-Field-Assisted Spectral Decomposition and Imaging of Charge States of N-*V* Centers in Diamond," *Physical Review Applied* 17 (2022): 024046.

Appendix

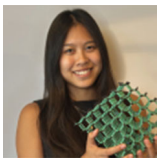
The anomalous data point at 548 nm laser wavelength and 95 K (Figure 5) is likely the result of laser power drift between measurements taken at the two bias magnetic field values. PL data is acquired in the following way: a cryostat temperature setpoint is entered, and while the cryostat is reaching a steady temperature the laser wavelength is set to the first value in the laser wavelength sweep. Once the laser wavelength locks and the temperature has stabilized, the system tunes the laser power to the power setpoint and changes the magnetic field to the initial reference value of 0 mT. When the laser power is at the setpoint, the power stabilizer software routine adjusts the power tuning polarizer's angle to maintain power at the setpoint. Once the laser power has been stable for 15 s, the spectrometer saves the reference PL spectrum with an overall exposure time of 1 s (100 ms exposure at 10 frame averages). When the spectrum is

18626319, 2026, 6, Downloaded from https://onlinelibrary.wiley.com/doi/10.1002/pssa.202500538 by Ronald Walsworth , Wiley Online Library on [16/03/2026]. See the Terms and Conditions (https://onlinelibrary.wiley.com/terms-and-conditions) on Wiley Online Library for rules of use; OA articles are governed by the applicable Creative Commons License

saved, the magnetic field is changed to the signal value of 100 mT. After a 5 s equilibration time, and if the laser power stability condition is still met, the spectrometer saves the signal PL spectrum. Normally this results in two PL spectra (reference and signal) taken at nearly identical laser powers; indeed the power stability condition is that the 15 s rolling average power must be within 0.25% of the set point. However, because the power stability setpoint is based on an average of 15 s of data taken at 50 ms intervals, a short-lived power excursion of a few percent will not violate the power stability condition. If this excursion occurs at the precise moment that one spectrum is being collected, that spectrum will be collected at a laser power that is at least a few percent different than the other PL spectrum. The result is that one spectrum is shifted up or down by a few percent in amplitude relative to the other, which can give the appearance of a large difference in contrast.

To detect these infrequent laser power excursions, two experimental heuristics are employed: C_{NV^-} does not depend strongly on excitation wavelength or temperature for wavelengths between 540 and 566 nm and for temperatures between 50 and 150 K [12]; and PL in the NV^- band exhibits a similar change to PL in the NV^0 band when the laser power changes, resulting in C_{NV^0} and C_{NV^-} changing by the same amount in the event of a power excursion. Comparing C_{NV^-} in a specific measurement to other values of C_{NV^-} at nearby temperatures and wavelengths can thus be used to distinguish C_{NV^0} outliers due to laser power excursions, e.g., the data point at 548 nm and 95 K (Figure 5).

Biographies



Kristine V. Ung is a fifth year Ph.D. student at the University of Maryland where she is a Joint Quantum Institute graduate research fellow. She has projects that focus on both the fundamental properties of defect charge configurations in diamonds and also the utilization of quantum diamond microscopes to identify physical phenomena in magnetic materials. This work follows a presentation she gave at the Hasselt Diamond Workshop in March 2025.



Sean M. Blakley is a research physicist and principle investigator in the Quantum Science & Technology branch at DEVCOM Army Research Laboratory and a former National Research Council postdoctoral research fellow in the Physical Measurement Laboratory at the National Institute of Standards & Technology. Sean's research is focused on investigating defects in solid state systems including diamond, silicon carbide, and others for use in quantum sensing.

18626319, 2026, 6, Downloaded from https://onlinelibrary.wiley.com/doi/10.1002/pssa.202500538 by Ronald Walsworth , Wiley Online Library on [16/03/2026]. See the Terms and Conditions (https://onlinelibrary.wiley.com/terms-and-conditions) on Wiley Online Library for rules of use; OA articles are governed by the applicable Creative Commons License